Valence-dependent analytic bond-order potential for transition metals

Ralf Drautz and D. G. Pettifor
Department of Materials, University of Oxford, Parks Road, Oxford OX1 3PH, United Kingdom
(Received 1 August 2006; published 21 November 2006)

An analytic interatomic bond-order potential is derived that depends explicitly on the valence of the transition-metal element. It generalizes the second-moment Finnis-Sinclair and fourth-moment Carlsson potentials to include higher moments. We find that the sixth-moment approximation predicts not only the structural trend from hcp→bcc→hcp→fcc that is observed across the nonmagnetic 4*d* and 5*d* transition-metal series, but also the different ferromagnetic moments of the bcc, fcc, and hcp phases of the 3*d* transition-metal iron. An analytic expression for the force is obtained and proved to converge to the Hellmann-Feynman force as higher moments are included.

DOI: 10.1103/PhysRevB.74.174117 PACS number(s): 71.20.Be, 75.50.Bb, 61.66.Bi

I. INTRODUCTION

The development of interatomic potentials that can model the very small energy differences between the various phases of transition metals and their alloys is key to the successful large-scale atomistic simulation of processes such as melting, amorphization, radiation induced defect cascades and subsequent defect clustering, and martensitic phase transitions.[1]

For the past two decades, the most widely used potentials for the atomistic simulation of metals have been the embedded-atom method (EAM) potentials[2,3] and the closely related Finnis-Sinclair (FS) potential.[4] The FS potential is derived from the second-moment approximation to the electronic density of states[5,6] and its resultant square-root embedding function is similar to the concave embedding function employed in EAM parametrizations. Both types of potentials may be classified as pair functionals.[7] It is now generally accepted, however, that the energy difference between crystal structures of transition metals is driven by higher moments than the second as the second moment only accounts for the root-mean-square width of the density of states (DOS) but is insensitive to changes in shape.[5,8] Therefore the second-moment approximation is unable to describe the competition between the fcc, bcc, and hcp phases of transition metals, and hence the observed trend across the nonmagnetic transition-metal series from hcp to bcc to hcp to fcc. Contributions of moments of order higher than 2 to the energy cannot be expressed in the form of pair functionals, thus the limitations of the second-moment approximation extend to pair functionals in general.

Several improvements to the second-moment potentials have been suggested that aim to cure their deficiencies by including higher moment contributions to the energy. Carlsson extended the second-moment approach by including the contributions of the fourth moment that cannot be represented as a pair functional.[9] Similarly, Hansen *et al.*[10] and Foiles[11] added an additional fourth-moment contribution to the EAM energy. These fourth-moment potentials have been successful in accounting for the sizeable stability of the bcc phase of the group-V and -VI transition metals compared to the metastable close-packed fcc and hcp phases which cannot be accounted for by the FS or EAM potentials.

However, the second-moment EAM- or FS-type potentials and their fourth-moment extensions are limited in their applicability by three key factors. First, the potentials are not easily extendable if improved accuracy is required. For example, in order that a potential is capable of predicting the stacking fault energy or the energy difference between the fcc and hcp structures, at least sixth-moment contributions are required.[8,12] None of the above potentials discusses the sixth-moment contributions. Second, the above potentials do not take into account the band-filling dependence of the effective interatomic interactions, whereas it is well known that this drives the observed structural trends across the periodic table.[8,13] Band-filling effects in these potentials are therefore implicitly contained in the parameters of a specific parametrization that has been fitted to reference data. An explicit understanding of the dependence of the fitting parameters on the band filling would improve the physical insight and therefore the robustness of a parametrization. Finally, the heat of formation of a transition-metal alloy is critically affected by the offset of the atomic *d* levels in the alloyed elements.[12,14,15] This offset is ignored in the second-moment models and their semiempirical fourth-moment extensions.

These limitations of the second-moment and fourth-moment interatomic potentials can be overcome by deriving the analytic form of the potentials directly by using perturbation theory with respect to the underlying electronic structure. During the 1980s Moriarty[16] applied generalized perturbation theory (GPT) to the *sp-d* bands of transition metals and obtained potentials for simple metals, noble metals, and transition metals. In 1990 he published a simplified variant of the GPT potential that expressed the many-atom interactions analytically.[17] The GPT potentials within the fourth-moment approximation have proved very successful in modeling defect behavior in nonmagnetic bcc transition metals.[18–20]

At the same time Haydock[21] and Turchi and Ducastelle[22] applied perturbation theory within the tight-binding (TB) recursion method. The resultant linear Green's-function method (LGM) has successfully explained structural and alloy trends across the transition-metal series.[22] Toward the end of the 1980s one of the current authors derived perturbatively an expression for the bond order[23] that subsequently developed in collaboration with Aoki[12,24–28] into an exact many-atom expansion for the bond-order potential (BOP). These BOPs have been applied by Vitek and his

collaborators[29–32] to a detailed study of dislocation behavior in transition metals and intermetallics. Unfortunately, these more fundamental approaches still required numerical integration of response functions, so that they were applicable to lattice static simulations but not molecular dynamics (MD). Alternatively, large scale MD simulations could be performed but then the prefactors of the various moment contributions were replaced by fitting parameters.

In this paper we derive analytic expressions for the response functions, bond energy, and forces that will allow us to perform MD simulations of transition metals and their alloys in the future. In Sec. II the TB model for the binding energy of transition metals is briefly introduced (Sec. II A), the concept of moments and many-atom expansion for the on-site bond energy discussed (Sec. II B), and a key BOP result presented that allows an intersite Green's function to be obtained from the derivative of an on-site Green's function (Sec. II C). In Sec. III analytic expressions are derived for the *on-site* density of states (Sec. III A), magnetic moments (Sec. III B), and bond energy (Sec. III C). We will see that retaining up to the sixth moment in the expansions is sufficient to explain both the different behavior of the ferromagnetic moments in 3*d*-valent iron between bcc and the close-packed phases under pressure, and also the structural trend from hcp→bcc→hcp→fcc across the nonmagnetic 4*d* and 5*d* transition-metal series. In Sec. IV analytic expansions are obtained for the *intersite* spectrally resolved density-matrix elements (Sec. IV A), bond order (Sec. IV B), and forces (Sec. IV C). We will show that the interatomic representation for the bond energy can be constrained to be identical to that within the on-site representation, and also that the analytic forces converge to the Hellmann-Feynman force as higher moments are included. In Sec. V we conclude.

II. TIGHT-BINDING REPRESENTATION OF THE BOND ENERGY

A. TB energy

A large number of papers on the basic formalism of tight-binding theory are available in the literature, see, for example, Ref. 33 and references therein. Here we only dicuss the aspects necessary for the development of analytic bond-order potentials for transition metals. We assume an orthonormal basis of atom-centered orbitals $|i\alpha\rangle$, where i is the atom index and α labels the five valence d orbitals on the atom. The matrix representation of the Hamiltonian is then given by the elements $H_{i\alpha j\beta}=\langle i\alpha|\hat{H}|j\beta\rangle$, which we take to be real valued. The diagonal or on-site matrix elements of the Hamiltonian are denoted by $E_{i\alpha}=H_{i\alpha i\alpha}$. The on-site matrix elements are identical, independent of the orbital α, if crystal-field effects are neglected, $E_i=E_{i\alpha}$.

Within the TB bond model the binding energy of nonmagnetic d-valent transition metals may then be written as the sum of repulsive and bond energies,[34]

$$U = U^{rep} + U^{bond}. \tag{1}$$

The repulsive contribution comprises a pairwise overlap repulsion and a short-ranged core term $U^{rep}=U^{pair}+U^{core}$,[29,30] whereas the attractive bond energy may be written in the form

$$U^{bond} = \sum_{i\alpha} 2\int^{E_F} (E-E_i)n_{i\alpha}(E)dE, \tag{2}$$

where the prefactor of 2 accounts for the spin degeneracy. The bond energy may be decomposed in terms of the contributions associated with each individual site, namely

$$U_i^{bond} = 10\int^{E_F} (E-E_i)n_i(E)dE, \tag{3}$$

where the average density of states $n_i(E)$ is defined by

$$n_i(E) = \frac{1}{5}\sum_{\alpha=1}^{5} n_{i\alpha}(E)dE. \tag{4}$$

Equation (2) gives the *on-site* representation of the total bond energy. Alternatively, this total bond energy may be expressed in terms of the off-diagonal elements of the density matrix $\rho_{i\alpha j\beta}$,

$$U^{bond} = \sum_{i\neq j}\sum_{\alpha\beta} 2\rho_{j\beta i\alpha}H_{i\alpha j\beta}. \tag{5}$$

This representation of the bond energy is called the *intersite* representation. The number of electrons in the orbital $|i\alpha\rangle$ is given by the diagonal elements of the density matrix $N_{i\alpha}=2\rho_{i\alpha i\alpha}=2\int^{E_F}n_{i\alpha}dE$.

The bond order measures the strength of a bond as the difference between the number of electrons in the bonding state N_+ and in the antibonding state N_-, respectively.[13,27] It is related to the density matrix by a factor of 2,

$$\Theta_{i\alpha j\beta} = \frac{1}{2}(N_+ - N_-) = 2\rho_{i\alpha j\beta}. \tag{6}$$

The density matrix $\rho_{i\alpha j\beta}$ may be expressed in terms of the single-particle Green's function G as

$$\rho_{i\alpha j\beta} = -\frac{1}{\pi}\,\mathrm{Im}\int^{E_F} G_{i\alpha j\beta}(E)dE. \tag{7}$$

Since the Green's-function operator $\hat{G}$ is defined by $(E-\hat{H})\hat{G}=\hat{1}$, it follows at once that the on-site expression Eq. (2) and the intersite expression Eq. (5) for the bond energy are identical.

B. On-site representation

The on-site representation for the bond energy Eq. (2) may be computed within an $O(N)$ approach by using the Lanczos algorithm[21,35] to evaluate the local electronic density of states. The algorithm transforms the original TB Hamiltonian matrix into the form of a semi-infinite one-dimensional nearest-neighbor chain by applying the recurrence relation

$$b_{n+1}|u_{n+1}\rangle = (\hat{H}-a_n)|u_n\rangle - b_n|u_{n-1}\rangle, \tag{8}$$

with $b_0=0$ and $|u_0\rangle=|i\alpha\rangle$, where the only nonvanishing matrix elements are given by

$$\langle u_m|\hat{H}|u_n\rangle = \begin{cases} a_n & \text{if } m=n, \\ b_n & \text{if } m=n-1, \\ b_{n+1} & \text{if } m=n+1. \end{cases} \tag{9}$$

Since the resultant Hamiltonian matrix with respect to the Lanczos orbitals is tridiagonal, the diagonal matrix element of the Green's function corresponding to the starting state $G_{00}=\langle u_0|\hat{G}|u_0\rangle=\langle u_0|(E-\hat{H})^{-1}|u_0\rangle$ may be immediately written as a continued fraction expansion,[35]

$$G_{00}(E) = \cfrac{1}{E-a_0-\cfrac{b_1^2}{E-a_1-\cfrac{b_2^2}{E-a_2-\cfrac{b_3^2}{\ddots}}}}. \tag{10}$$

As the starting Lanczos orbital $|u_0\rangle$ has been chosen as the appropriate atomic orbital $|i\alpha\rangle$, the local density of states is given by $n_{i\alpha}(E)=-\frac{1}{\pi}\,\mathrm{Im}\,G_{00}(E)$.

The recursion coefficients $\{a_n,b_n\}$ that enter the continued fraction for the local density of states $n_{i\alpha}(E)$ may be expressed directly in terms of the moments of the density of states $\mu_{i\alpha}^{(n)}$, where

$$\mu_{i\alpha}^{(n)} = \int E^n n_{i\alpha}(E)dE. \tag{11}$$

As is well known, the zeroth moment $\mu_{i\alpha}^{(0)}=1$ corresponds to the maximum number of electrons with given spin that may occupy the orbital $|i\alpha\rangle$, the first moment $\mu_{i\alpha}^{(1)}$ defines the center of gravity of the local density of states, the second moment $\mu_{i\alpha}^{(2)}$ measures its mean square width, the third moment $\mu_{i\alpha}^{(3)}$ and fourth moment $\mu_{i\alpha}^{(4)}$ its skewness and bimodality, respectively. An important identity relates the moment $\mu_{i\alpha}^{(n)}$ to all possible hopping paths of length n that start and end on orbital $|i\alpha\rangle$,[5,36]

$$\mu_{i\alpha}^{(n)} = \sum_{i_1\alpha_1,i_2\alpha_2,\ldots,i_{n-1}\alpha_{n-1}} \langle i\alpha|\hat{H}|i_1\alpha_1\rangle \times\langle i_1\alpha_1|\hat{H}|i_2\alpha_2\rangle\cdots\langle i_{n-1}\alpha_{n-1}|\hat{H}|i\alpha\rangle. \tag{12}$$

Thus by taking $|u_0\rangle=|i\alpha\rangle$ as the starting orbital along the semi-infinite Lanczos chain, it is straightforward to write the moments as functions of the recursion coefficients a_n and b_n^2, so that, for example,

$$\mu_{i\alpha}^{(0)}=1, \quad \mu_{i\alpha}^{(1)}=0, \quad \mu_{i\alpha}^{(2)}=b_1^2, \quad \mu_{i\alpha}^{(3)}=a_1b_1^2, \quad \text{and}$$

$$\mu_{i\alpha}^{(4)} = b_1^2b_2^2+b_1^4+a_1^2b_1^2, \tag{13}$$

where for simplicity we have taken the on-site energy $E_i=a_0$ as the energy zero. It follows that the recursion coefficients may be expressed in terms of the moments as

$$b_1^2=\mu_{i\alpha}^{(2)}, \quad a_1=\mu_{i\alpha}^{(3)}/\mu_{i\alpha}^{(2)}, \quad \text{and}$$

$$b_2^2=(\mu_{i\alpha}^{(4)}/\mu_{i\alpha}^{(2)})-(\mu_{i\alpha}^{(3)}/\mu_{i\alpha}^{(2)})^2-\mu_{i\alpha}^{(2)}. \tag{14}$$

Thus b_1 is a measure of the root-mean-square width, a_1 is the skewing, and b_2 is the bimodality of the density of states. The latter follows directly from Eq. (10) since the continued fraction comprises only two poles for $b_2=0$.

The average local density of states $n_i(E)$ may be obtained from Eq. (10) by evaluating the corresponding recursion coefficients $\{a_n,b_n\}$ from the average moments,

$$\mu_i^{(n)} = \int E^n n_i(E)dE = \frac{1}{5}\sum_{\alpha=1}^{5}\mu_{i\alpha}^{(n)}. \tag{15}$$

Therefore both the local density of states and the on-site bond energy may be computed within an $O(N)$ real-space approach.[37,38] This methodology has been implemented in the standard Oxford $O(N)$ (OXON) package.[27,28]

An important many-atom expansion for the local on-site bond energy has been derived by Aoki, initially indirectly using BOP theory [see Eq. (23) of Ref. 26] and later directly using the properties of the Green's function $G_{0n}=\langle u_0|\hat{G}|u_n\rangle$ defined along the semi-infinite Lanczos chain [see Eq. (B11) of Ref. 39]. The expansion takes the form

$$U_i^{bond} = 10\sum_{n=1}^{\infty}\{\chi_{2n}(E_F)[b_n^2-b_{n-1}^2]+\chi_{2n+1}(E_F)[(a_n-a_{n-1})b_n]\}, \tag{16}$$

where the response functions are defined by

$$\chi_m = \begin{cases} -\dfrac{1}{\pi}\,\mathrm{Im}\displaystyle\int^{E_F} G_{0[(m-2)/2]}G_{[(m-2)/2]0}dE & \text{for } m \text{ even}, \\ -\dfrac{1}{\pi}\,\mathrm{Im}\displaystyle\int^{E_F} G_{0[(m-3)/2]}G_{[(m-1)/2]0}dE & \text{for } m \text{ odd}. \end{cases} \tag{17}$$

The prefactor 10 in Eq. (16) is a consequence of this bond energy arising from all five d orbitals on site i with spin up and spin down. Note that the recursion coefficients $\{a_n,b_n\}$ and hence the Lanczos chain Green's functions G_{0n} are implicitly dependent on the site i through the average moments $\mu_i^{(n)}$.

Contact can now be made with both the second-moment[4–6] and fourth-moment[9–11] expressions for the bond energy. Simplifying Eq. (16) by neglecting odd moment contributions through setting $a_n=0$ and keeping only the first two terms in the resultant expansion, we find

$$U_i^{bond} = 10\sqrt{\mu_i^{(2)}}\{\hat{\chi}_2(\phi_F)+\hat{\chi}_4(\phi_F)[\mu_i^{(4)}/(\mu_i^{(2)})^2-2]\}, \tag{18}$$

using the relationship between recursion coefficients and moments given by Eq. (14). The $\hat{\chi}$ are the reduced response functions introduced in the original BOP paper,[23] being defined to be dimensionless through $\hat{\chi}_n=\chi_n/\sqrt{\mu_i^{(2)}}$. They take a simple analytic form[23] under the approximation $b_n=b_1$ and $a_n=0$ when

$$\hat{\chi}_n(\phi_F) = \frac{1}{\pi}\left(\frac{\sin(n+1)\phi_F}{n+1}-\frac{\sin(n-1)\phi_F}{n-1}\right), \tag{19}$$

where $\phi_F=\cos^{-1}[E_F/(2b_1)]$ for $n\geqslant 2$.

We see immediately from Eq. (18) that the first term corresponds to the second-moment contribution of the Finnis-Sinclair potential,[4] whereas the second term corresponds to the fourth-moment contribution introduced by Carlsson.[9] Importantly, however, Eq. (18) also contains prefactors that are valence dependent through the Fermi energy E_F. Unfortunately, Alinaghian *et al.*[40] found that the simplest approximation for the response functions given by Eq. (19) leads to poor structural prediction as can be seen from the $b_2=b_1$ curve in their Fig. 2. On the other hand, they showed that using the correct value of b_2 in Eq. (16) leads to good agreement[40] with the fourth-moment TB results of Brown and Carlsson[41] but involves extremely complicated *analytic* expressions[42] for the two response functions $\hat{\chi}_2[(b_2/b_1),E_F]$ and $\hat{\chi}_4[(b_2/b_1),E_F]$. One of the goals of this paper is to derive an analytic expression for the on-site bond energy that is physically transparent and easy to use in MD simulations of transition metals and their alloys. This will be pursued in Sec. III A once we have addressed the intersite representation for the bond energy.

C. Intersite representation

Unlike the on-site representation, the intersite representation allows a decomposition of the bond energy associated with a given atom in terms of the individual contributions from its neighboring bonds. This provides physical and chemical insights into the weakening or strengthening of bonds due to, for example, the presence of nearby defects or impurities. It also provides a procedure for calculating the force on a given atom k directly by using the Hellmann-Feynman theorem[43,44] which states that

$$\boldsymbol{F}_k^{bond} = -\sum_{i\neq j}\sum_{\alpha\beta}(\nabla_k H_{i\alpha j\beta})\Theta_{j\beta i\alpha}, \tag{20}$$

since $\Theta=2\rho$ by Eq. (6). This deceptively simple expression appears to give the force for "free" once the bond order has been calculated because the gradient of the TB Hamiltonian matrix elements are straightforward to evaluate. Unfortunately, the bond orders are very poorly converged if they are computed directly from Eq. (6) as the difference between the numbers of occupied bonding and antibonding states. This led to the development of BOP theory during the late 1980s and early 1990s as an attempt to obtain a rapidly convergent $O(N)$ method for evaluating the intersite Green's function and hence the intersite density matrix or bond order.[12,23–26]

A key result of BOP theory[25] is that the intersite Green's function $G_{i\alpha j\beta}$ can be written as the derivative of an on-site Green's function which as we have seen in Eq. (2) can be expressed as a well-behaved continued fraction. This can be proved very simply. Let us take the starting Lanczos orbital $|u_0^\lambda\rangle$ as an admixture of the relevant orbitals on the two sites i and j, namely

$$|u_0^\lambda\rangle = c_{i\alpha}|i\alpha\rangle + c_{j\beta}e^{i\vartheta}|j\beta\rangle, \tag{21}$$

where $\lambda=\cos\vartheta$ and $c_{i\alpha}^2+c_{j\beta}^2=1$. Then

$$G_{00}^\lambda = \langle u_0^\lambda|(E-\hat{H})^{-1}|u_0^\lambda\rangle = c_{i\alpha}^2 G_{i\alpha i\alpha} + c_{j\beta}^2 G_{j\beta j\beta} + 2c_{i\alpha}c_{j\beta}\lambda G_{i\alpha j\beta}. \tag{22}$$

Hence the intersite Green's function $G_{i\alpha j\beta}$ can be written as the derivative of the diagonal Green's function G_{00}^λ as

$$G_{i\alpha j\beta} = \frac{1}{2c_{i\alpha}c_{j\beta}}\frac{dG_{00}^\lambda}{d\lambda}. \tag{23}$$

In conventional BOP theory[23,26,27] $G_{00}^\lambda = G_{00}^\lambda(\{a_n^\lambda, b_n^\lambda\})$ from Eq. (10), so that

$$G_{i\alpha j\beta} = \frac{1}{2c_{i\alpha}c_{j\beta}}\left(\sum_{n=0}^{\infty}\frac{\partial G_{00}^\lambda}{\partial a_n^\lambda}\frac{\partial a_n^\lambda}{\partial\lambda} + \sum_{n=1}^{\infty}\frac{\partial G_{00}^\lambda}{\partial b_n^\lambda}\frac{\partial b_n^\lambda}{\partial\lambda}\right). \tag{24}$$

Performing the partial derivatives and substituting the resultant intersite Green's function with $\lambda=0$ into Eq. (7), an *exact* many-atom expansion for the bond order may be derived, namely,

$$\Theta_{i\alpha j\beta} = 2\sum_{n=1}^{\infty}(\chi_{2n}\delta a_{n-1}^{i\alpha j\beta} + \chi_{2n+1}\delta b_n^{i\alpha j\beta}), \tag{25}$$

where the Lanczos chain response functions have already been defined in Eq. (17). The coefficients $\{\delta a_n, \delta b_n\}$ depend on the interference paths $\xi_{i\alpha j\beta}^{(m)}=\langle i\alpha|\hat{H}^m|j\beta\rangle$ that link the atomic orbitals $|i\alpha\rangle$ and $|j\beta\rangle$ [see, for example, Eqs. (2.26)–(2.30) of Ref. 12]. Substituting this expression for the bond order, or intersite density-matrix element, into Eq. (5) leads to a many-body expression for the intersite bond energy.

In practice, the on-site and intersite expressions for the bond energy are evaluated using a Lanczos chain that is exact only up to some given level $n_{max}/2$ by setting $a_{n-1}=a_\infty$ and $b_n=b_\infty$ for $n>n_{max}/2$ (that is, all moments μ_n are exact up to $\mu_{n_{max}}$, Ref. 45). It is clear that this approximation to the tail of the Lanczos chain will lead to the many-atom expansion for the bond energy Eq. (16) within the *on-site* representation, terminating after $n=n_{max}/2-1$. In 1993 Aoki[26] showed that by suitably truncating the many-body expansion for the bond order within the *intersite* representation the resultant bond energy Eq. (5) could be made identical to that for the on-site representation at any level of approximation n_{max}. This methodology of *numerical* BOPs has been implemented in the standard OXON package, where the bond orders or intersite density-matrix elements are used to determine the forces directly by using the Hellmann-Feynman theorem.[27] However, due to the slow convergence of the Hellmann-Feynman forces, this approach has to date only been applied to nondynamic simulations.[29–32] In the following sections we introduce a different approach that leads to *analytic* expressions for the local density of states, bond energies, and forces.

III. ON-SITE EXPANSIONS

A. Density of states

The simplest approximation to the average on-site density of states $n_i(E)$ is to assume that the recursion coefficients

take constant values $a_n=a_{i\infty}$, $b_n=b_{i\infty}$ all the way along the Lanczos chain (see Sec. 12 of Ref. 21). This results in a semielliptic density of states $n_{i0}(E)=n_{i0}(\epsilon)/(2b_{i\infty})$ where

$$n_{i0}(\epsilon) = \frac{2}{\pi}\sqrt{1-\epsilon^2}, \tag{26}$$

with $\epsilon=(E-a_{i\infty})/(2b_{i\infty})$. We see that this represents a single band of states between $\epsilon=\pm 1$ and $E=a_{i\infty}\pm 2b_{i\infty}$. The second-moment approximation corresponds to taking $a_{i\infty}=a_{i0}$, $b_{i\infty}=b_{i1}$, so that the resultant bond energy is proportional to b_{i1} or the square root of the second moment about site i.[4]

In this paper the second-moment approximation is extended by writing the local density of states in the form[21,22]

$$n_i(\epsilon) = n_{i0}(\epsilon) + \delta n_i(\epsilon). \tag{27}$$

The semielliptic behavior of $n_{i0}(\epsilon)$ suggests expanding $\delta n_i(\epsilon)$ in terms of Chebyshev polynomials of the second kind[46] $P_n(\epsilon)$ since they are orthonormal with respect to the weight function $\frac{2}{\pi}\sqrt{1-\epsilon^2}$, that is

$$\frac{2}{\pi}\int_{-1}^{1} P_n(\epsilon)P_m(\epsilon)\sqrt{1-\epsilon^2}d\epsilon = \delta_{nm}. \tag{28}$$

Thus we write

$$n_i(\epsilon) = \frac{2}{\pi}\sqrt{1-\epsilon^2}\left(1+\sum_{m=0}\tilde{\sigma}_i^{(m)}P_m(\epsilon)\right). \tag{29}$$

The Chebyshev polynomials of the second kind satisfy the recurrence relation

$$P_{m+1}(\epsilon) = 2\epsilon P_m(\epsilon) - P_{m-1}(\epsilon), \tag{30}$$

with $P_0(\epsilon)=1$ and $P_1(\epsilon)=2\epsilon$. Since $P_0(\epsilon)=1$, we have

$$n_i(\epsilon) = \frac{2}{\pi}\sqrt{1-\epsilon^2}\sum_{m=0}\sigma_i^{(m)}P_m(\epsilon), \tag{31}$$

where $\sigma^{(0)}=1+\tilde{\sigma}^{(0)}$ and $\sigma^{(m)}=\tilde{\sigma}^{(m)}$ for $m\neq 0$.

A similar expansion of the density of states employing Chebyshev polynomials of the first kind is used in the kernel polynomial method.[47–49] However, the Chebyshev polynomials of the first kind are orthogonal with respect to the weight function $\frac{2}{\pi}\frac{1}{\sqrt{1-\epsilon^2}}$ and therefore are not well adapted to a systematic extension of the second moment density of states Eq. (27), while the Chebyshev polynomials of the second kind, which we use, are the eigenstates of the semi-infinite constant Lanczos chain[21] and therefore are well suited for the expansion of the density of states of transition metals.

The coefficients $\sigma_i^{(m)}$ are given by

$$\sigma_i^{(m)} = \int_{-1}^{1} P_m(\epsilon)n_i(\epsilon)d\epsilon. \tag{32}$$

They may be expressed in terms of the dimensionless moments $\hat{\mu}_i^{(n)}$ of the density of states $n_i(\epsilon)=(2b_{i\infty})n_i(E)$, namely

TABLE I. Dimensionless moments $\hat{\mu}_i^{(m)}$ for $m=0,1,\ldots,6$ as a function of parameters γ_n and δ_n. The second and third columns give exact and linear expressions, respectively.

	Exact	Linear
$\hat{\mu}_i^{(0)}$	1	1
$2\hat{\mu}_i^{(1)}$	γ_0	γ_0
$2^2\hat{\mu}_i^{(2)}$	$1+\gamma_0^2$	1
$2^3\hat{\mu}_i^{(3)}$	$2\gamma_0+\gamma_0^3$	$2\gamma_0$
$2^4\hat{\mu}_i^{(4)}$	$2+3\gamma_0^2+\gamma_0^4+\delta_2$	$2+\delta_2$
$2^5\hat{\mu}_i^{(5)}$	$5\gamma_0+4\gamma_0^3+\gamma_0^5+\gamma_2+2\gamma_0\delta_2+\gamma_2\delta_2$	$5\gamma_0+\gamma_2$
$2^6\hat{\mu}_i^{(6)}$	$\begin{bmatrix} 5+9\gamma_0^2+5\gamma_0^4+\gamma_0^6+2\gamma_0\gamma_2+\gamma_2^2+5\delta_2 \\ +3\gamma_0^2\delta_2+2\gamma_0\gamma_2\delta_2+\gamma_2^2\delta_2+\delta_2^2+\delta_3+\delta_2\delta_3 \end{bmatrix}$	$5+5\delta_2+\delta_3$

$$\hat{\mu}_i^{(n)} = \int_{-1}^{1}\epsilon^n n_i(\epsilon)d\epsilon. \tag{33}$$

Expanding the Chebyshev polynomials in Eq. (32) explicitly as

$$P_m(\epsilon) = \sum_{n=0}^{m} p_{mn}\epsilon^n, \tag{34}$$

where the p_{mn} satisfy the recursion relation

$$p_{(m+1)n} = 2p_{m(n-1)} - p_{(m-1)n}, \tag{35}$$

with $p_{mn}=0$ if $n<0$ or $n>m$, we find that

$$\sigma_i^{(m)} = \sum_{n=0}^{m} p_{mn}\hat{\mu}_i^{(n)}. \tag{36}$$

The dimensionless moments $\hat{\mu}_i^{(n)}$ may be obtained directly from the moments $\mu_i^{(n)}$ of the average local density of states $n_i(\epsilon)$. Substituting $\epsilon=(E-a_{i\infty})/(2b_{i\infty})$ into Eq. (33) and performing the binomial expansion, we have

$$\hat{\mu}_i^{(n)} = \frac{1}{(2b_{i\infty})^n}\sum_{l=0}^{n}\binom{n}{l}(-1)^l a_{i\infty}^l \mu_i^{(n-l)}. \tag{37}$$

We expect these expansion coefficients $\sigma_i^{(m)}$ for $m\neq 0$ to vanish for the special case of the constant Lanczos chain with $a_n=a_{i\infty}$, $b_n=b_{i\infty}$. This is confirmed by defining new variables,

$$\gamma_{in} = (a_{in}-a_{i\infty})/b_{i\infty}, \quad \delta_{in} = (b_{in}^2-b_{i\infty}^2)/b_{i\infty}^2, \tag{38}$$

and using the relationship Eq. (14) between the moments and the Lanczos recursion coefficients. Note that we have chosen these variables because $G_{00}(E)$ in Eq. (10) is a function of $\{a_n,b_n^2\}$.

The resultant expressions for the normalized moments $\hat{\mu}_i^{(n)}$ and the expansion coefficients $\sigma_i^{(n)}$ are given in Tables I and II, respectively, for $n=0,1,\ldots,6$. We see that the $\sigma_i^{(m)}$ indeed vanish for $m\neq 0$ for the constant Lanczos chain with

TABLE II. Expansion coefficients $\sigma_i^{(n)}$ for $n=0,1,\ldots,6$ as a function of γ_n and δ_n.

	Exact	Linear
$\sigma_i^{(0)}$	1	1
$\sigma_i^{(1)}$	γ_0	γ_0
$\sigma_i^{(2)}$	γ_0^2	0
$\sigma_i^{(3)}$	γ_0^3	0
$\sigma_i^{(4)}$	$\gamma_0^4+\delta_2$	δ_2
$\sigma_i^{(5)}$	$\gamma_0^5+\gamma_2+2\gamma_0\delta_2+\gamma_2\delta_2$	γ_2
$\sigma_i^{(6)}$	$\gamma_0^6+3\gamma_0^2\delta_2+\delta_2^2+2\gamma_0\gamma_2(1+\delta_2)+\gamma_2^2(1+\delta_2)+\delta_3+\delta_2\delta_3$	δ_3

$\gamma_{in}=0$, $\delta_{in}=0$. Moreover, $\sigma_i^{(0)}$ is always unity so that the first term in the expansion for $\delta n_i(\epsilon)$ in Eq. (29) will drop out in general as $\tilde{\sigma}_i^{(0)}=0$.

The local density of states $n_i(\epsilon)$ can therefore be expanded in terms of the Chebyshev polynomials of the second kind as

$$n_i^{(n_{max})}(\epsilon)=\frac{2}{\pi}\sqrt{1-\epsilon^2}\sum_{m=0}^{n_{max}}\sum_{n=0}^{m}p_{mn}\hat{\mu}_i^{(n)}P_m(\epsilon), \tag{39}$$

where we have introduced the upper summation limit n_{max} to indicate the largest exact moment $\hat{\mu}_i^{(n_{max})}$ included in the expansion. Because the expansion is linear with respect to the moments of the density of states, this expansion may also be used to calculate the orbital resolved density of states,

$$n_{i\alpha}^{(n_{max})}(\epsilon)=\frac{2}{\pi}\sqrt{1-\epsilon^2}\sum_{m=0}^{n_{max}}\sum_{n=0}^{m}p_{mn}\hat{\mu}_{i\alpha}^{(n)}P_m(\epsilon), \tag{40}$$

with

$$\hat{\mu}_{i\alpha}^{(n)}=\frac{1}{(2b_{i\infty})^n}\sum_{l=0}^{n}\binom{n}{l}(-1)^l a_{i\infty}^l\mu_{i\alpha}^{(n-l)}. \tag{41}$$

We will make use of Eq. (40) in the derivation of the expressions for the bond order in Sec. IV A.

The rate of convergence of the infinite series as $n_{max}\rightarrow\infty$ will be dependent upon the choice of the reference density of states $n_{i0}(\epsilon)$. Although the choice of $a_{i\infty}$ and $b_{i\infty}$ could be optimized for each atom at each step in an MD simulation using input from all the exact moments or recursion coefficients,[50] our goal in this paper is to derive simple analytic expressions for the densities of states, bond energies, and forces. We will see from Fig. 4 in the next section that choosing $a_{i\infty}=a_{i1}$ and $b_{i\infty}=b_{i1}$ leads to a sufficiently accurate convergence of the resultant bond energy provided we take $n_{max}=6$ and include up to the sixth moment, μ_6, exactly. Moreover, the choice of $b_{i\infty}=b_{i1}$ guarantees that the local density of states $n_i(E)$ scales as the inverse of b_1, thereby retaining the spirit of the second-moment approximation. In addition, the choice of $a_{i\infty}=a_{i1}$ partially reflects the asymmetry of the band edges with respect to the on-site energy that is always present in close-packed metallic systems due to the many three-body rings and resultant self-returning three hop contributions to the third moment.[8]

We have evaluated the *d*-band density of states for the bcc, fcc, and ideal hcp structures within the sixth-moment expansion corresponding to $n_{max}=6$, assuming that $a_\infty=a_1$ and $b_\infty=b_1$, where we have dropped the site indices as all sites are equivalent. The calculations were carried out using canonical bond integrals $dd\sigma:dd\pi:dd\delta=-6:4:-1$.[51] First-nearest neighbors only were retained for the fcc and ideal hcp structures, whereas for bcc second-nearest neighbors were also included assuming that the bond integrals fall off with distance as the inverse fifth power.[52] The bcc bond integrals were scaled to guarantee that the second moment $\mu^{(2)}$ of the average bcc density of states was identical to that for fcc and hcp.[8] Table III gives the resultant values of γ_n and δ_n, the dimensionless moments $\hat{\mu}^{(n)}$ and the expansion coefficients $\sigma^{(n)}$, respectively. We find that δ_1 and γ_1 are identically zero for all three structures due to our choice of $b_\infty=b_1$ and $a_\infty=a_1$, respectively.

The upper panel in Fig. 1 compares the densities of states of bcc, fcc, and hcp within the sixth-moment expansion corresponding to $n_{max}=6$ using the *exact* expressions for the moments that are given in Table I. As expected, we see that the bcc density of states is much more bimodal than the close-packed structures fcc and hcp due to its value of δ_2 in Table III being more negative than for either fcc or hcp. On the other hand, the two close-packed structures have very similar values of δ_n and γ_n for $n\leqslant 2$, the first significant difference being δ_3 where hcp takes a negative value but fcc a positive value in Table III. Since δ_3 only affects the expansion coefficient $\sigma^{(6)}$ in Table II, it follows from Eq. (31) that there will be a difference in the sixth-order Chebyshev polynomials $P_6(\epsilon)$ contribution in the density of states. This ac-

TABLE III. Numerical values of expansion parameters γ_n and δ_n, the dimensionless moments $\hat{\mu}_i^{(n)}$, and exact coefficients $\sigma_i^{(n)}$ for sixth-moment expansion in bcc, fcc, and hcp structures.

	bcc	fcc	hcp		bcc	fcc	hcp		bcc	fcc	hcp
γ_0	0.232	0.240	0.240	$\hat{\mu}_i^{(1)}$	0.116	0.120	0.120	$\sigma_i^{(1)}$	0.232	0.240	0.240
δ_1	0.000	0.000	0.000	$\hat{\mu}_i^{(2)}$	0.263	0.264	0.264	$\sigma_i^{(2)}$	0.054	0.058	0.058
γ_1	0.000	0.000	0.000	$\hat{\mu}_i^{(3)}$	0.060	0.062	0.062	$\sigma_i^{(3)}$	0.013	0.014	0.014
δ_2	−0.371	−0.231	−0.235	$\hat{\mu}_i^{(4)}$	0.112	0.122	0.121	$\sigma_i^{(4)}$	−0.369	−0.227	0.232
γ_2	0.156	−0.123	−0.129	$\hat{\mu}_i^{(5)}$	0.036	0.033	0.033	$\sigma_i^{(5)}$	−0.074	−0.205	−0.211
δ_3	0.399	0.009	−0.123	$\hat{\mu}_i^{(6)}$	0.063	0.068	0.066	$\sigma_i^{(6)}$	0.389	−0.014	−0.114

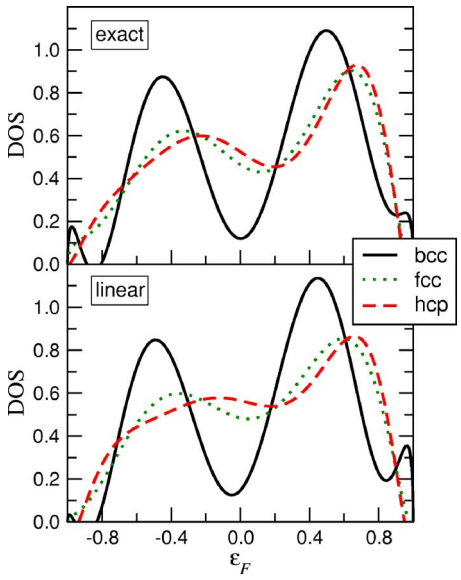

FIG. 1. (Color online) Comparison of bcc, fcc, and ideal hcp *d*-band densities of states within sixth-moment expansion. Curves in upper and lower panels were evaluated using exact and linear expressions for expansion coefficients in Table II, respectively.

counts for the fcc and hcp curves crossing each other six times in Fig. 1 between the bottom and top of the bands. Finally, we should point out that as might be expected from polynomial expansions, the density of states display unphysical negative values. However, these are only observed very close to the band edges and with small absolute values, so that they will not interfere with any treatment of groups III–VIII transition metals and their alloys.

The lower panel compares the densities of states for $n_{max}=6$ using the *approximate* expressions for the moments that include only the linear terms with respect to γ_n and δ_n, as given in the right-hand column of Table I. The corresponding values of the expansion coefficients $\sigma^{(n)}$ in Table II lead to the following simple form of the density of states:

$$n_i^{(n_{max}L)}(\epsilon)=\frac{2}{\pi}\sqrt{1-\epsilon^2}\left(1+\sum_{m=0}^{n_{max}/2}[\gamma_{im}P_{2m+1}(\epsilon)+\delta_{i(m+1)}P_{2m+2}(\epsilon)]\right), \tag{42}$$

where the superscript L denotes that the linear approximation has been made and for generality we have reintroduced the site indices for systems with nonequivalent sites. This is consistent with the first-order Dyson equation for the Lanczos chain Green's function $\mathrm{Im}\,G_{00}$ when the constant chain is perturbed by on-site energy shifts $(a_{im}-a_{i\infty})/(2b_{i\infty})$ and intersite hopping integral shifts $(b_{im}-b_{i\infty})/(2b_{i\infty})$ since to first order $\delta_{im}=4(b_{im}-b_{i\infty})/(2b_{i\infty})$. This first-order expansion for the density of states has been discussed previously by Haydock[21] and Turchi and Ducastelle.[22] Importantly, however, using the exact expansion coefficients, Eq. (39) maintains the linear dependence of the density of states on the dimensionless moments $\hat{\mu}_i^{(n)}$ that we will see is central to the equivalence of our on-site and intersite energy expressions. We observe in Fig. 1 that this approximate form does an excellent job in reflecting the different behavior of the exact bcc, fcc, and hcp curves within the sixth-moment expansion.

Although, as is well known, the density of states converges very slowly with respect to the number of exact moments retained, integrated quantities converge much faster,[21,52] as we will see in the next two subsections.

B. Magnetic moments

Magnetism plays an important role in determining the structure and properties of some 3*d* transition-metal elements. In particular, iron's phase diagram shows all three common metallic structures bcc (α and δ phases), fcc (γ phase), and hcp (ϵ phase) as a function of temperature and pressure.[53] We might have expected Fe to behave more like the nonmagnetic isovalent 4*d* element Ru and the 5*d* element Os which are hcp in their ground states. But the narrow 3*d* band and high peak in the density of states at the Fermi level in nonmagnetic iron help to stabilize a large magnetic moment and drive the bcc phase to be more stable than the nonmagnetic hcp phase at low temperatures and pressure. This very different behavior in the magnetic moments of bcc, hcp, and fcc iron is due to the dependence of the magnetic moments on the shape of the nonmagnetic density of states in the vicinity of the Fermi level.

This dependence follows directly from the Stoner model of itinerant magnetism[54] which predicts the self-consistent ferromagnetic moment is determined by the condition[55–58]

$$I\bar{n}_s(E_F)=1, \tag{43}$$

where I is the Stoner exchange integral and $\bar{n}_s(E_F,m)$ is the average density of states *per spin* between the down-spin and up-spin Fermi levels when the down-spin electrons are flipped about the initial nonmagnetic Fermi level E_F to create a spin imbalance m. Thus the Stoner condition requires an integral over the nonmagnetic density of states, namely

$$\bar{n}_s(E_F,m)=\frac{\int_{E_F^\downarrow}^{E_F^\uparrow}n_s(E)dE}{E_F^\uparrow-E_F^\downarrow}=\frac{m}{E_F^\uparrow-E_F^\downarrow}, \tag{44}$$

where $m=N^\uparrow-N^\downarrow$. The self-consistent value of the magnetic moment is then obtained by finding the value of m in Eq. (44) such that $\bar{n}_s(E_F)=1/I$ from Eq. (43).

Within canonical *d*-band theory the shape of the density of states remains unaltered as the volume changes, so that the Stoner condition, Eq. (43) may be rewritten[57,58] in terms of the dimensionless density of states per spin $n_s(\epsilon)$, namely

$$[I/(2b_1)]\bar{n}_s(\epsilon_F,m)=1, \tag{45}$$

where $2b_1=W/2$ is half the bandwidth. The variation of the resultant self-consistent magnetic moment with normalized exchange integral $I/(2b_1)$ for $N_d=7$ corresponding to iron is plotted in the left-hand panel of Fig. 2 using the highly accurate linear tetrahedron method to evaluate the density of states. We see that canonical Stoner theory predicts that the magnetic moment of bcc iron decreases gradually with de-

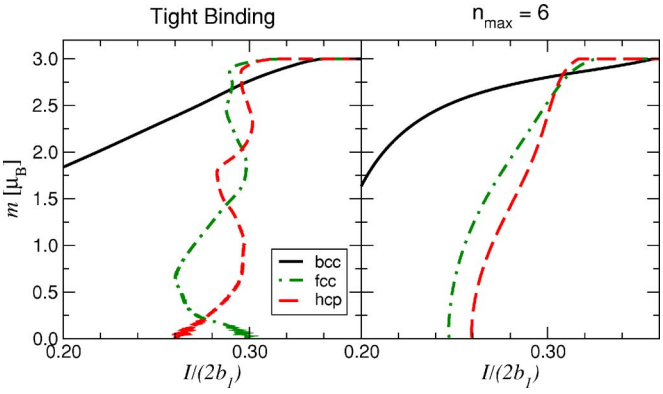

FIG. 2. (Color online) Variation of bcc, fcc, and hcp ferromagnetic moments m with normalized Stoner exchange integral $I/(2b_1)$ for $N=7$ corresponding to iron. In the left-hand panel the $\boldsymbol{k}$-space linear tetrahedron method was used to evaluate the TB density of states, whereas in the right-hand panel $n_{max}=6$ expansion was used, Eq. (39).

creasing normalized exchange integral (or volume), whereas the two close-packed structures fcc and hcp initially fall precipitously at some critical value of normalized exchange integral (or volume). These $\boldsymbol{k}$-space TB predictions, first made 30 years ago,[57,58] were later confirmed by first-principles density-functional theory (see, for example, Ref. 59).

The right-hand panel of Fig. 2 shows the predicted variation of the magnetic moments using the expansion Eq. (31) of the density of states and the resultant band occupancy for up and down spins with $n_{max}=6$. It follows from Eq. (31) using $\sqrt{1-\epsilon^2}P_n(\epsilon)=\sin[(n+1)\phi]$ that the *total* number of electrons per atom on site i, N_i, is given by

$$N_i(\phi_F) = 10\sum_{m=0}^{n_{max}} \sigma_i^{(m)} \hat{\chi}_{m+1}(\phi_F), \tag{46}$$

where

$$\hat{\chi}_1 = 1 - \frac{\phi_F}{\pi} + \frac{1}{2\pi}\sin(2\phi_F) \tag{47}$$

and $\hat{\chi}_{m+1}(\phi_F)$ has already been defined in Eq. (19) for $m>0$. Thus the magnetic moment $m=N^{\uparrow}-N^{\downarrow}$ can be expressed as

$$m_i = 5\sum_{m=0}^{n_{max}} \sigma_i^{(m)}[\hat{\chi}_{m+1}(\epsilon_F^{\uparrow}) - \hat{\chi}_{m+1}(\epsilon_F^{\downarrow})]. \tag{48}$$

We see from the right-hand panel in Fig. 2 that the resultant self-consistent moments reproduce the very different magnetic behavior of bcc and the two close-packed phases. As explained in Refs. 57 and 58 this is due to the nonmagnetic Fermi level falling near the top of the broad right-hand peak of the bcc density of states in Fig. 1, whereas the Fermi levels of fcc and hcp fall halfway down the slope. Clearly the sixth-moment expansion is unable to reproduce the oscillations in the fcc and hcp TB curves that are observed in the left-hand panel. These are intimately related through Eq. (45) to the fine structure of the density of states such as local peaks or troughs[57,58] which are smoothed out in the sixth-moment expansion.

Choosing a value of $I=0.63$ eV (Ref. 60) and $W=5$ eV (Ref. 61) for iron at its equilibrium volume would lead to a normalized exchange integral of 0.25, which can account from Fig. 2 for the experimental observation that bcc iron is ferromagnetic with a large moment but hcp iron is nonmagnetic. Second-moment models[62,63] can account for the local volume dependence of the magnetic moments but they cannot predict the structural variation that depends explicitly on the shape of the density of states. In the next subsection we derive the expansion for the bond energy of *nonmagnetic* systems. We will return to the *magnetic* contribution to the binding energy in a future publication.

C. Bond energy

The bond energy associated with atom i can be written from Eq. (3) as

$$U_i^{bond} = 20 b_{i\infty}\int_{-1}^{\epsilon_F} (\epsilon - \gamma_{i0}/2) n_i(\epsilon) d\epsilon, \tag{49}$$

where $\epsilon=(E-a_{i\infty})/(2b_{i\infty})$. Substituting in the expansion for the density of states, Eq. (31), and using the recurrence relation for $\epsilon P_m(\epsilon)$ given by Eq. (30), we find

$$U_i^{bond(n_{max})} = 10 b_{i\infty}\sum_{m=0}^{n_{max}} \sigma_i^{(m)} \int_{-1}^{\epsilon_F} \frac{2}{\pi}\sqrt{1-\epsilon^2}[P_{m+1}(\epsilon) - \gamma_{i0}P_m(\epsilon) + P_{m-1}(\epsilon)] d\epsilon. \tag{50}$$

Substituting $\epsilon=\cos\phi$ and $\sqrt{1-\epsilon^2}P_m(\epsilon)=\sin[(m+1)\phi]$ into the above equation, we obtain

$$U_i^{bond(n_{max})} = 10 b_{i\infty}\sum_{m=0}^{n_{max}} \sigma_i^{(m)}[\hat{\chi}_{m+2}(\phi_F) - \gamma_{i0}\hat{\chi}_{m+1}(\phi_F) + \hat{\chi}_m(\phi_F)], \tag{51}$$

where the reduced response functions are defined in Eqs. (19) and (47) for $m\neq 0$ and $\chi_0=0$. This expression can be simplified by substituting in the *exact* values of the expansion coefficients $\sigma_i^{(2)}$ and $\sigma_i^{(3)}$ in Table II for $a_{i\infty}=a_{i1}$, $b_{i\infty}=b_{i1}$. We find

$$U_i^{bond(n_{max})} = 10 b_{i1}\left(\hat{\omega}_2(\phi_F) + \gamma_{i0}\hat{\omega}_3(\phi_F) + \sum_{m=4}^{n_{max}} \sigma_i^{(m)}\hat{\omega}_m(\phi_F)\right), \tag{52}$$

where

$$\hat{\omega}_2(\phi_F) = \hat{\chi}_2(\phi_F), \tag{53}$$

$$\hat{\omega}_3(\phi_F) = \gamma_{i0}^2\hat{\chi}_5(\phi_F) + \gamma_{i0}(1-\gamma_{i0}^2)\hat{\chi}_4(\phi_F) + \hat{\chi}_3(\phi_F), \tag{54}$$

$$\hat{\omega}_m(\phi_F) = \hat{\chi}_{m+2}(\phi_F) - \gamma_{i0}\hat{\chi}_{m+1}(\phi_F) + \hat{\chi}_m(\phi_F). \tag{55}$$

Further, if the expansion coefficients are approximated by

their *linearized* values in Table II, then Eq. (52) reduces to

$$U_i^{bond(n_{max})} = 10b_{i1}\left(\hat{U}_{i0}^{bond}(\phi_F) + \sum_{m=2}^{n_{max}/2} \delta_{im}\hat{\omega}_{2m}(\phi_F) + \sum_{m=2}^{n_{max}/2-1} \gamma_{im}\hat{\omega}_{2m+1}(\phi_F)\right), \quad (56)$$

where $\hat{U}_{i0}^{bond}(\phi_F)$ is the dimensionless bond energy of the reference Lanczos chain within the linear approximation. It is given by

$$\hat{U}_{i0}^{bond}(\phi_F) = \hat{\omega}_2(\phi_F) + \gamma_{i0}\hat{\omega}_3(\phi_F). \quad (57)$$

Within the symmetric fourth-moment approximation this expression simplifies to

$$U_i^{(bond)}/(10\sqrt{\mu_i^{(2)}}) = \hat{\chi}_2(\phi_F) + [\hat{\chi}_4(\phi_F) + \hat{\chi}_6(\phi_F)] \times [\mu_i^{(4)}/(\mu_i^{(2)})^2 - 2]. \quad (58)$$

We see that this looks similar to our earlier expression, Eq. (18), for the bond energy. Importantly, however, the prefactor for the fourth-moment contribution is not simply $\hat{\chi}_4$ as in Eq. (18) but $(\hat{\chi}_4+\hat{\chi}_6)$, the additional response function $\hat{\chi}_6$ arising from the $(b_2/b_1)^2$ dependence in the exact response function $\chi_2[(b_2/b_1), E_F]$ in Eq. (17). For half full bands (corresponding to $\phi_F=\pi/2$) the new prefactor $(\hat{\chi}_4+\hat{\chi}_6)$ takes a value of 0.061 compared to the old $\hat{\chi}_4$ prefactor value of 0.170.[40] The new slope agrees very well with the slope of the line in the Brown-Carlsson plot[41] of normalized TB bond energy vs fourth moment for *s*-valent structures containing no odd-membered rings.

The convergence of the bond-energy expansion, Eq. (52), with respect to higher moments is illustrated in Fig. 3. This shows the band filling dependence of the bond energy for the reference Lanczos chain to first order and the further five contributions ($n=4-8$) for bcc, fcc, and hcp. We see that the reference contribution is an order of magnitude larger than other contributions and varies almost parabolically with band filling. Thus the influence of the third moment is small and accounts for the second-moment approximation[5,6,8] providing a good explanation for the observed variation of the cohesive energies across the nonmagnetic 4*d* and 5*d* transition-metal series.

The differentiation of the relative structural stability of bcc, fcc, and hcp requires moments higher than third. We see that the fourth-moment contribution ($n=4$) favors the bcc structure over the close-packed in the vicinity of half full bands whereas the close-packed structures are favored toward the band edges, as observed in practice across the nonmagnetic transition-metal series. This behavior due to the presence of two nodes in the $n=4$ curves reflects the increased bimodality of the bcc density of states compared to fcc and hcp in Fig. 1. We observe that differentiation of the close-packed structures requires the sixth-moment contribution ($n=6$) whose curves display four nodes, as expected from the moment theorem of Ducastelle and Cyrot-Lackmann.[64] This contribution correctly predicts that

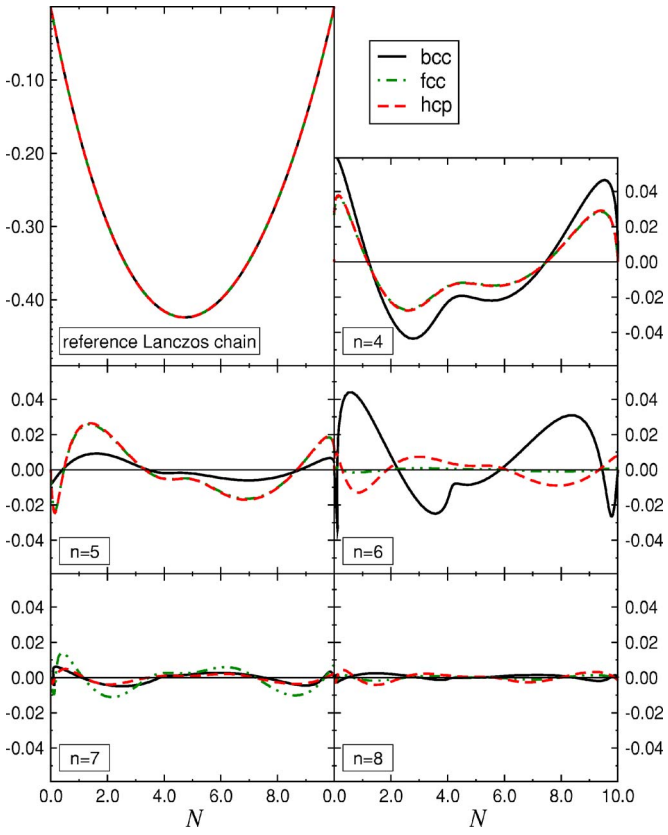

FIG. 3. (Color online) Dimensionless bond energy contributions for reference Lanczos chain and the next five contributions ($n=4-8$) for bcc, fcc, and hcp as function of band filling.

away from half full bands the bcc phase gives way on either side to the hcp phase. We see that that contributions from $n=7$ and $n=8$ are small.

Figure 4 shows explicitly the convergence of the (bcc-fcc) and (hcp-fcc) energy differences as the number of moments is increased. We see that the fourth-moment approximation indeed stabilizes bcc for half full bands, whereas the sixth-moment contribution is required to differentiate fcc and hcp. We also observe for these crystalline metallic systems that the linear and first-order approximations to the expansion coefficients reproduce reasonably well the results from using the exact coefficients in Table II. Thus our analytic *d*-valent BOPs are able to converge to sufficient accuracy by $n_{max}=6$ to reproduce energy differences that are of the order of less than 1% of the cohesive energy. In particular, they predict the observed structural trend from hcp→bcc→hcp→fcc across the nonmagnetic transition-metal series (apart from $N=9$ corresponding to Pd and Pt, where the *sp-d* hybridization contribution is dominant[8]).

IV. INTERSITE EXPANSION

A. Spectrally resolved density matrix

In Sec. II C we saw from Eq. (23) that BOP theory expresses the off-diagonal Green's-function matrix elements $G_{i\alpha j\beta}$ as the derivative with respect to the phase of the diagonal Green's-function matrix element $G_{00}^{\lambda}=\langle u_0^{\lambda}|\hat{G}|u_0^{\lambda}\rangle$, where

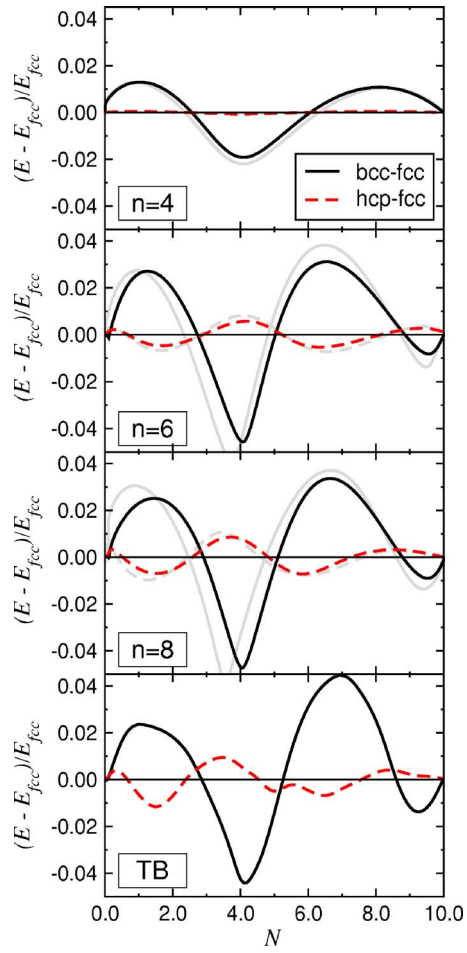

FIG. 4. (Color online) Convergence of (bcc-fcc) and (hcp-fcc) normalized energy differences as the number of moments is increased using exact expressions (dark curves) and linear expressions (light curves) for expansion coefficients. Energies have been normalized with respect to fcc bond energy at half full band.

$|u_0^\lambda\rangle$ is the starting Lanczos orbital, Eq. (21), comprising an admixture of orbitals on site i and j. Unlike numerical BOP theory[25] where G_{00}^λ is considered as a function of the recursion coefficients $\{a_n, b_n\}$ as in Eq. (24), in the present analytic approach we will consider G_{00}^λ as a function of the moments $\{\mu_0^{(n)}(\lambda)\}$ where from Eq. (21) $\mu_0^{(n)}(\lambda)=\langle u_0^\lambda|\hat{H}^n|u_0^\lambda\rangle$ is given by

$$\mu_0^{(n)}(\lambda) = c_{i\alpha}^2\mu_{i\alpha}^{(n)} + c_{i\beta}^2\mu_{i\beta}^{(n)} + 2\lambda c_{i\alpha}c_{j\beta}\xi_{i\alpha j\beta}^{(n)}. \tag{59}$$

Thus using Eq. (23) we can write

$$G_{i\alpha j\beta}(E) = \sum_n \frac{1}{2c_{i\alpha}c_{j\beta}}\frac{\partial G_{00}(E)}{\partial \mu_0^{(n)}}\frac{\partial \mu_0^{(n)}}{\partial \lambda} = \sum_n \xi_{i\alpha j\beta}^{(n)}\frac{\partial G_{00}(E)}{\partial \mu_0^{(n)}}. \tag{60}$$

This intersite Green's function is different from the numerical BOP in that it is independent of $c_{i\alpha}$ and $c_{j\beta}$. The convergence of the expansion therefore is independent of the choice of starting orbital $|u_0^\lambda\rangle$ whether an atom-based orbital or a bond-based state is used.[39]

Written in terms of the dimensionless energy $\epsilon=(E-a_\infty)/(2b_\infty)$, this equation reads

$$G_{i\alpha j\beta}(\epsilon) = \sum_n \frac{1}{2c_{i\alpha}c_{j\beta}}\frac{\partial G_{00}(\epsilon)}{\partial \hat{\mu}_0^{(n)}}\frac{\partial \hat{\mu}_0^{(n)}}{\partial \lambda} = \sum_n \hat{\xi}_{i\alpha j\beta}^{(n)}\frac{\partial G_{00}(\epsilon)}{\partial \hat{\mu}_0^{(n)}}, \tag{61}$$

where the dimensionless interference paths are given by

$$\hat{\xi}_{i\alpha j\beta}^{(l)} = \sum_{n=0} \xi_{i\alpha j\beta}^{(n)}\frac{\partial \hat{\mu}_0^{(l)}}{\partial \mu_0^{(n)}} = \frac{1}{(2b_\infty)^l}\sum_{n=0}^{l}\binom{n}{l}(-a_\infty)^{n-l}\xi_{i\alpha j\beta}^{(n)}, \tag{62}$$

with $\xi_{i\alpha j\beta}^{(0)}=0$ for $|i\alpha\rangle \neq |j\beta\rangle$. The definition of $\hat{\xi}^{(n)}$ in Eq. (62) is analogous to that of the dimensionless moments in Eq. (33). The upper limit of the summation in Eq. (62) is due to $\frac{\partial \hat{\mu}_{i\alpha}^{(n)}}{\partial \hat{\mu}_{i\alpha}^{(l)}}=0$ for $l>n$.

Assuming $a_\infty=a_{i\infty}$ and $b_\infty=b_{i\infty}$ to be site dependent and taking the expansion of Eq. (61) only to a finite number of moments n_{max} will in general break the Hermiticity of $G_{i\alpha j\beta}$. For finite n_{max}, we therefore use an explicitly symmetric form of $G_{i\alpha j\beta}^{(n_{max})}$,

$$\bar{G}_{i\alpha j\beta}^{(n_{max})}(E) = \frac{1}{2}[G_{i\alpha j\beta}^{(n_{max})}(E) + G_{j\beta i\alpha}^{(n_{max})}(E)], \tag{63}$$

where here and in the following a_∞ and b_∞ are taken from the first index of G, i.e., $G_{i\alpha j\beta}^{(n_{max})}=G_{i\alpha j\beta}^{(n_{max})}(a_{i\infty}, b_{i\infty})$ and $G_{j\beta i\alpha}^{(n_{max})}=G_{j\beta i\alpha}^{(n_{max})}(a_{j\infty}, b_{j\infty})$.

The spectrally resolved density-matrix element $n_{i\alpha j\beta}=-\frac{1}{\pi}\mathrm{Im}G_{i\alpha j\beta}$ can therefore be written as

$$\bar{n}_{i\alpha j\beta}(E) = \frac{1}{2}[n_{i\alpha j\beta}(E) + n_{j\beta i\alpha}(E)], \tag{64}$$

where $n_{i\alpha j\beta}(E)=n_{i\alpha j\beta}(\epsilon)/(2b_{i\infty})$. Including moments up to n_{max}, it follows from Eq. (40) that

$$n_{i\alpha j\beta}^{(n_{max})}(\epsilon) = \frac{2}{\pi}\sqrt{1-\epsilon^2}\sum_{m=0}^{n_{max}}\sigma_{i\alpha j\beta}^{(m)}P_m(\epsilon), \tag{65}$$

where

$$\sigma_{i\alpha j\beta}^{(m)} = \sum_{n=0}^{m} p_{mn}\hat{\xi}_{i\alpha j\beta}^{(n)}. \tag{66}$$

The definition of $\sigma_{i\alpha j\beta}^{(m)}$ is analogous to the definition of the expansion coefficients $\sigma_i^{(m)}$ in Eq. (32).

We now examine the constraint on the spectrally resolved density matrix for the on-site and intersite bond energies resulting from Eqs. (39) and (65) to be equivalent. These two different representations are guaranteed to be identical if the integral kernels of the on-site expansion, Eq. (2), and intersite expansion, Eq. (5), are the same for each atom,[24] that is,

$$(E-E_i)n_i^{(n_{max})}(E) = \frac{1}{5}\sum_{j\neq i}\sum_{\alpha\beta}H_{i\alpha j\beta}n_{i\alpha j\beta}^{(n_{max})}(E). \tag{67}$$

In reduced units $\epsilon=(E-a_{i\infty})/(2b_{i\infty})$ this equivalence reads

$$(\epsilon - \gamma_{i0}/2)n_i^{(n_{max})}(\epsilon) = \frac{1}{5}\sum_{j\neq i}\sum_{\alpha\beta} h_{i\alpha j\beta} n_{i\alpha j\beta}^{(n_{max})}(\epsilon), \tag{68}$$

where $h_{i\alpha j\beta}=H_{i\alpha j\beta}/(2b_{i\infty})$. The left-hand side of Eq. (68) may be rewritten by inserting the expansion for the density of states, Eq. (31), and using the Chebyshev recurrence relation Eq. (30), so that

$$\kappa^{(on)} = \frac{1}{\pi}\sqrt{1-\epsilon^2}\sum_{m=0}^{n_{max}} \sigma_i^{(m)}[P_{m+1}(\epsilon) - \gamma_{i0}P_m(\epsilon) + P_{m-1}(\epsilon)]. \tag{69}$$

As expected, we find that the uppermost expansion coefficient that enters the summation corresponds to $m=n_{max}$.

On the other hand, the right-hand side of Eq. (68) may be rewritten by inserting the expansion for the spectrally resolved density matrix, Eq. (65), so that

$$\kappa^{(inter)} = \frac{2}{\pi}\sqrt{1-\epsilon^2}\sum_{m=0}^{n_{max}}\sum_{n=0}^{m} p_{mn}\left(\hat{\mu}_i^{(n+1)} - \frac{\gamma_{i0}}{2}\hat{\mu}_i^{(n)}\right)P_m(\epsilon), \tag{70}$$

since

$$\frac{1}{5}\sum_{j\neq i}\sum_{\alpha\beta} h_{i\alpha j\beta}\hat{\xi}_{i\alpha j\beta}^{(n)} = \hat{\mu}_i^{(n+1)} - \frac{\gamma_{i0}}{2}\hat{\mu}_i^{(n)}. \tag{71}$$

Equation (70) may be further simplified by taking into account that

$$\sum_{n=0}^{m} p_{mn}\hat{\mu}^{(n+1)} = \int_{-1}^{1} \epsilon P_m(\epsilon) n_i(\epsilon) d\epsilon = \frac{1}{2}[\sigma_i^{(m+1)} + \sigma_i^{(m-1)}], \tag{72}$$

where the first equality follows from Eq. (34) and the second equality from Eqs. (30) and (32). Hence

$$\kappa^{(inter)} = \kappa^{(on)} + \frac{1}{\pi}\sqrt{1-\epsilon^2}[\sigma_i^{(n_{max})}P_{n_{max}+1}(\epsilon) - \sigma_i^{(n_{max}+1)}P_{n_{max}}(\epsilon)]. \tag{73}$$

We find therefore that the uppermost expansion coefficient that enters the intersite kernel is $m=n_{max}+1$. This is not totally unexpected since we have obtained the intersite kernel in Eq. (70) via a single multiplication of the Hamiltonian matrix with the spectral function.

Thus our constraint on the definition of the spectrally resolved intersite density-matrix element is that the additional factor in the square brackets of Eq. (73) must vanish. This can be achieved most simply and robustly by adding a constraint contribution to Eq. (65),

$$\Delta n_{i\alpha j\beta}^{(n_{max})}(\epsilon) = \frac{1}{\pi}\sqrt{1-\epsilon^2}\hat{\zeta}_{i\alpha j\beta}[\sigma_i^{(n_{max}+1)}P_{n_{max}}(\epsilon) - \sigma_i^{(n_{max})}P_{n_{max}+1}(\epsilon)], \tag{74}$$

where

$$\hat{\zeta}_{i\alpha j\beta} = \frac{1}{n_{max}}\sum_{n=1}^{n_{max}} \frac{\hat{\xi}_{i\alpha j\beta}^{(n)}}{\hat{\mu}_i^{(n+1)} - (\gamma_{i0}/2)\hat{\mu}_i^{(n)}}. \tag{75}$$

Substituting Eqs. (74) and (75) into the right-hand side of Eq. (68), premultiplying by the Hamiltonian matrix elements and summing over j, α, and β, we see that we achieve the exact cancellation of the second term on the right-hand side of Eq. (73). In the next section we will find that this choice of terminator leads to only small additional contributions to the bond order while guaranteeing the equivalence of the on-site and intersite representation for the bond energy.

B. Bond order

The bond order between orbitals on different atoms i and j may be obtained directly from integrating the spectrally resolved density-matrix element up to the Fermi energy. We find

$$\bar{\Theta}_{i\alpha j\beta} = \frac{1}{2}[\Theta_{i\alpha j\beta} + \Theta_{j\beta i\alpha}], \tag{76}$$

where

$$\Theta_{i\alpha j\beta}^{(n_{max})} = 2\left\{\sum_{m=1}^{n_{max}} \sigma_{i\alpha j\beta}^{(m)}\hat{\chi}_{m+1}(\phi_F) + \hat{\zeta}_{i\alpha j\beta}[\sigma_i^{(n_{max}+1)}\hat{\chi}_{n_{max}+1}(\phi_F) - \sigma_i^{(n_{max})}\hat{\chi}_{n_{max}+2}(\phi_F)]\right\}. \tag{77}$$

The prefactor 2 accounts for the spin degeneracy in nonmagnetic systems and the second contribution inside the curly brackets results from integrating the constraint contribution Eq. (75). The expansion coefficients $\sigma_{i\alpha j\beta}^{(m)}$ depend explicitly on the interference paths through Eq. (66). These paths are illustrated diagrammatically in Fig. 2 of Ref. 12. If we take into account only the leading diagram for each order within the ring approximation[12] and neglect the constraint contribution, then expansion Eq. (77) is identical to Eq. (17) of the original BOP paper.[23]

Figure 5 compares the resultant bond orders for bcc, fcc, and hcp within the sixth-moment approximation corresponding to $n_{max}=6$ with $\boldsymbol{k}$-space TB results. We see that our constrained bond-order expression reproduces the TB results extremely well, including the fine details between the in-plane and out-of-plane bond orders in the hcp structure. The unconstrained sixth-moment approximation also reproduces the TB results well, introducing only a small contribution that is visible for the bcc π bond order in the top right-hand panel of Fig. 5. This shows that the constraint contribution is indeed small.

C. Forces

The forces resulting from the bond-energy expansion may be evaluated with an effort similar to the evaluation of Hellmann-Feynman forces.[43,44] It follows from Eq. (49) that for the particular case where a_∞ and b_∞ are chosen to be site independent, the gradient of the bond energy is given by

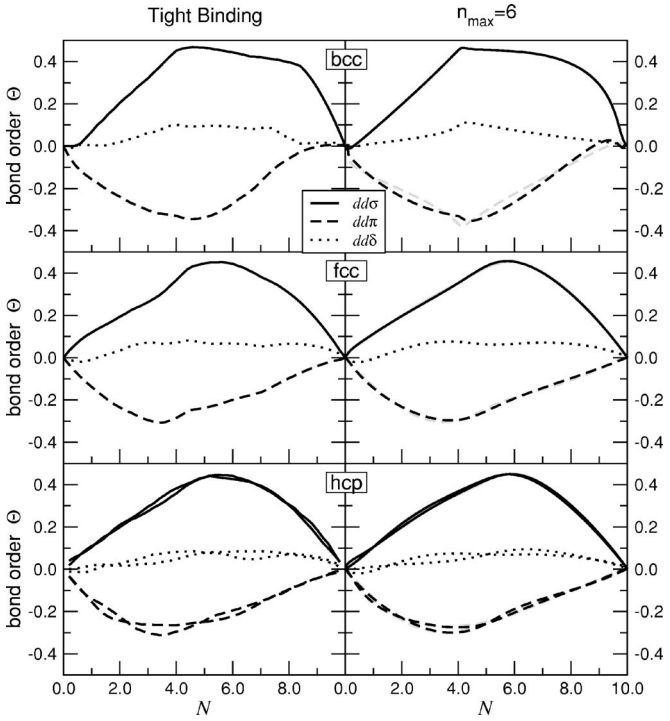

FIG. 5. Comparison of first nearest-neighbor σ, π, and δ bond orders within sixth-moment approximation with $\boldsymbol{k}$-space TB results for bcc, fcc, and hcp as a function of the d valence. Dark (light) curves correspond to Eq. (76) with (without) constraint contribution. As the latter contribution is small, light curves are visible only for bcc π bond order.

$$\nabla_k U^{bond} = 20 b_\infty \sum_i \int_{-1}^{\epsilon_F} (\epsilon - 1/2\,\gamma_{i0}) \nabla_k n_i(\epsilon) d\epsilon$$

$$= 20 b_\infty \int_{-1}^{\epsilon_F} \epsilon \sum_i \nabla_k n_i(\epsilon) d\epsilon. \quad (78)$$

The second equality follows because we have made the excellent approximation for metals that each atom remains locally charge neutral, so that $\nabla_k N_i$ vanishes. Substituting the expansion for the density of states, Eq. (39), the gradient becomes

$$\nabla_k U^{bond(n_{max})} = 10 b_\infty \sum_{m=0}^{n_{max}} \sum_{n=0}^{m} p_{mn} \nabla_k \sum_i \hat{\mu}_i^{(n)} \times [\hat{\chi}_{m+2}(\phi_F) + \hat{\chi}_m(\phi_F)]. \quad (79)$$

The derivative of the dimensionless moments $\nabla_k \hat{\mu}_i^{(n)}$ may be further simplified,

$$\nabla_k \sum_i \hat{\mu}_i^{(n)} = \frac{1}{5} \sum_{i\alpha} \langle i\alpha | \nabla_k \hat{h}^n | i\alpha \rangle$$

$$= \frac{1}{5} \sum_{i\alpha} \langle i\alpha | n \hat{h}^{n-1} \nabla_k \hat{h} | i\alpha \rangle$$

$$= \frac{1}{5} \sum_{i\alpha j\beta} n \hat{\xi}_{i\alpha j\beta}^{(n-1)} \nabla_k h_{j\beta i\alpha}, \quad (80)$$

where $\hat{h} = (\hat{H} - a_\infty)/(2b_\infty)$ and we have taken into account that the trace of a product of operators is invariant with respect to cyclic exchange of arguments. Finally, by introducing

$$\tilde{\Theta}_{i\alpha j\beta}^{(n_{max})} = 2 \sum_{m=0}^{n_{max}} \sum_{n=0}^{m} p_{mn} n \hat{\xi}_{i\alpha j\beta}^{(n-1)} [\hat{\chi}_{m+2}(\phi_F) + \hat{\chi}_m(\phi_F)], \quad (81)$$

with $\hat{\xi}_{i\alpha j\beta}^{(-1)} = 0$, the forces may be written in a form similar to Hellmann-Feynman forces,

$$\boldsymbol{F}_k^{bond} = -\nabla_k U^{bond(n_{max})} = -\sum_{i\alpha j\beta} \tilde{\Theta}_{i\alpha j\beta}^{(n_{max})} (\nabla_k H_{j\beta i\alpha}). \quad (82)$$

We prove in the Appendix that as n_{max} tends to infinity, $\tilde{\Theta}^{(n_{max})} \to \Theta$, so that we recover the exact Hellmann-Feynman force Eq. (20). It remains for future research to investigate the magnitude of the errors made by using site-dependent coefficients $a_{i\infty}$ and $b_{i\infty}$ in our analytic BOP expansion.

V. CONCLUSION

In this paper we have derived analytic expressions for the bond energy and forces within d-valent transition-metal systems. This has been achieved by expanding the on-site density of states in terms of Chebyshev polynomials of the second kind weighted by the semielliptic density of states corresponding to the well-known second-moment approximation. The resulting expansion generalizes the second-moment approximation to the density of states by including higher moments that enter the expansion linearly. We showed using Stoner theory that including contributions up to the sixth moment in the density of states was sufficient to reproduce the very different behavior observed between the ferromagnetic moments of bcc $3d$-valent iron and its close-packed fcc and hcp phases under pressure. The corresponding sixth-moment expansion for the bond energy associated with a given site was also found to display the hcp $\to$ bcc $\to$ hcp $\to$ fcc structural trend across the nonmagnetic $4d$ and $5d$ transition-metal series.

We have derived an analytic expression for the bond order by using BOP theory to write the intersite Green's function as a derivative of an on-site Green's function. The resultant expansion coefficients are linear combinations of the interference paths that link the atoms at the two ends of the bond. We showed that the corresponding intersite representation for the bond energy can be constrained to be identical to that within the on-site representation. An analytic expression for the forces is obtained in terms of a linear combination of the interference paths. It is proved to converge to the Hellmann-Feynman force as higher moments are included.

These analytic BOPs not only generalize the previous second-moment Finnis-Sinclair and fourth-moment Carlsson potentials to include higher moments, but they also give explicit analytic expressions for the valence dependence of the prefactors associated with the different moment contributions. Thus they are applicable to both the study of property trends across the transition-metal elements and alloy behavior. These potentials are currently being fitted to bcc transition metals in order to perform large scale MD simulations of

defect evolution under high-energy neutron bombardment in fusion reactors.

ACKNOWLEDGMENTS

R.D. and D.G.P. would like to acknowledge the hospitality of the IPAM long workshop at UCLA on *Bridging Time and Length Scales in Materials Science and Bio-Physics* in the Fall of 2005 where most of the key results of this paper were derived. We would also like to thank our collaborators within the EPSRC funded project on *Predictive modelling of mechanical properties of materials for fusion power plants* for throwing down the challenge of obtaining a robust analytic interatomic potential for transition metals and their alloys. We would like to thank Tony Paxton for providing at short notice his code for the accurate TB DOS integration in Fig. 2. R.D. would like to thank DARPA/ONR for partial support of the initial research under the Research Contract No. GG10551-119199.

APPENDIX: CONVERGENCE TO HELLMANN-FEYNMAN FORCE

In this Appendix we show that $\tilde{\Theta}_{i\alpha j\beta}^{(n_{max})}$ as defined in Eq. (81) converges to the bond order for $n_{max}\rightarrow\infty$. We start by rewriting the interference paths in terms of the eigenstates $|k\rangle$,

$$\hat{h}|k\rangle = \epsilon_k|k\rangle, \tag{A1}$$

with $\hat{h}=(\hat{H}-a_\infty)/(2b_\infty)$, so that

$$\hat{\xi}_{i\alpha j\beta}^{(n)} = \langle i\alpha|\hat{h}^n|j\beta\rangle = \sum_k \langle i\alpha|k\rangle\epsilon_k^n\langle k|j\beta\rangle. \tag{A2}$$

The derivative of the interference paths may be written as

$$\sum_k \frac{\partial}{\partial\epsilon_k}\hat{\xi}_{i\alpha j\beta}^{(n)} = \sum_k n\langle i\alpha|k\rangle\epsilon_k^{n-1}\langle k|j\beta\rangle = n\hat{\xi}_{i\alpha j\beta}^{(n-1)}. \tag{A3}$$

Therefore Eq. (81) becomes

$$\tilde{\Theta}_{i\alpha j\beta}^{(n_{max})} = 2\sum_k \frac{\partial}{\partial\epsilon_k}\left(\sum_{m=0}^{n_{max}}\sum_{n=0}^{m} p_{mn}\hat{\xi}_{i\alpha j\beta}^{(n)}\int^{\epsilon_F}\epsilon P_m(\epsilon)\right). \tag{A4}$$

Substituting Eqs. (65) and (66), this may be rewritten as

$$\tilde{\Theta}_{i\alpha j\beta}^{(n_{max})} = 2\sum_k \frac{\partial}{\partial\epsilon_k}\int^{\epsilon_F}\epsilon n_{i\alpha j\beta}^{(n_{max})}(\epsilon)d\epsilon. \tag{A5}$$

Taking the limit $n_{max}\rightarrow\infty$ and making use of the spectral representation of $n_{i\alpha j\beta}(\epsilon)$,[27]

$$n_{i\alpha j\beta}(\epsilon) = \sum_l \langle i\alpha|l\rangle\langle l|j\beta\rangle\delta(\epsilon-\epsilon_l), \tag{A6}$$

the above equation becomes

$$\tilde{\Theta}_{i\alpha j\beta} = 2\sum_l\sum_k \frac{\partial}{\partial\epsilon_k}\int^{\epsilon_F}\epsilon\langle i\alpha|l\rangle\langle l|j\beta\rangle\delta(\epsilon-\epsilon_l)d\epsilon, \tag{A7}$$

$$= 2\sum_l^{occupied}\sum_k \frac{\partial}{\partial\epsilon_k}\epsilon_l\langle i\alpha|l\rangle\langle l|j\beta\rangle, \tag{A8}$$

$$= 2\sum_l^{occupied}\sum_k \delta_{lk}\langle i\alpha|l\rangle\langle l|j\beta\rangle, \tag{A9}$$

$$= 2\sum_l^{occupied}\langle i\alpha|l\rangle\langle l|j\beta\rangle, \tag{A10}$$

$$= \Theta_{i\alpha j\beta}. \tag{A11}$$

Hence our analytic expression for the forces, Eq. (82), tends to the Hellmann-Feynman result as $n_{max}\rightarrow\infty$.

[1] *Handbook of Materials Modelling*, edited by S. Yip (Springer, New York, 2005).
[2] M. S. Daw and M. I. Baskes, Phys. Rev. Lett. **50**, 1285 (1983).
[3] M. S. Daw and M. I. Baskes, Phys. Rev. B **29**, 6443 (1984).
[4] M. W. Finnis and J. E. Sinclair, Philos. Mag. A **50**, 45 (1984).
[5] F. Ducastelle and F. Cyrot-Lackmann, J. Phys. Chem. Solids **31**, 1295 (1970).
[6] G. Allan and M. Lannoo, J. Phys. Chem. Solids **37**, 699 (1976).
[7] A. E. Carlsson, in *Solid State Physics: Advances in Research and Applications*, edited by H. Ehrenreich and D. Turnbull (Academic, Boston, 1990), Vol. 43.
[8] D. G. Pettifor, *Bonding and Structure in Molecules and Solids* (Oxford University Press, Oxford, 1995).
[9] A. E. Carlsson, Phys. Rev. B **44**, 6590 (1991).
[10] L. Hansen, P. Stoltze, K. W. Jacobsen, and J. K. Norskov, Phys. Rev. B **44**, 6523 (1991).
[11] S. M. Foiles, Phys. Rev. B **48**, 4287 (1993).
[12] D. G. Pettifor and M. Aoki, Philos. Trans. R. Soc. London, Ser. A **334**, 439 (1991).
[13] R. Drautz and M. Fähnle, Phys. Rev. B **72**, 212405 (2005).
[14] D. G. Pettifor, Phys. Rev. Lett. **42**, 846 (1979).
[15] F. Ducastelle, *Order and Phase Stability in Alloys* (North-Holland, Amsterdam, 1991).
[16] J. A. Moriarty, Phys. Rev. B **38**, 3199 (1988).
[17] J. A. Moriarty, Phys. Rev. B **42**, 1609 (1990).
[18] J. A. Moriarty, Phys. Rev. B **49**, 12431 (1994).
[19] J. A. Moriarty, V. Vitek, V. V. Bulatov, and S. Yip, J. Comput.-Aided Mater. Des. **9**, 99 (2002a).
[20] J. A. Moriarty, J. F. Belak, R. E. Rudd, P. Söderlind, F. H. Streitz, and L. H. Yang, J. Phys.: Condens. Matter **14**, 2825 (2002b).
[21] R. Haydock, Solid State Phys. **35**, 216 (1980).
[22] P. E. A. Turchi and F. Ducastelle, in *The Recursion Method and its Applications*, Springer Series in Solid State Sciences Vol. 58, edited by D. G. Pettifor and D. L. Weaire (Springer, Berlin,

1985), p. 104.
[23] D. G. Pettifor, Phys. Rev. Lett. **63**, 2480 (1989).
[24] M. Aoki and D. G. Pettifor, Int. J. Mod. Phys. B **7**, 299 (1993a).
[25] M. Aoki and D. G. Pettifor, in *International Conference on the Physics of Transition Metals: Darmstadt, Germany, July 20–24, 1992*, edited by P. M. Oppeneer and J. K. Kübler (World Scientific, Singapore, 1993), p. 299.
[26] M. Aoki, Phys. Rev. Lett. **71**, 3842 (1993).
[27] A. P. Horsfield, A. M. Bratkovsky, M. Fearn, D. G. Pettifor, and M. Aoki, Phys. Rev. B **53**, 12694 (1996a).
[28] A. P. Horsfield, A. M. Bratkovsky, D. G. Pettifor, and M. Aoki, Phys. Rev. B **53**, 1656 (1996b).
[29] S. Znam, D. Nguyen-Manh, D. G. Pettifor, and V. Vitek, Philos. Mag. **83**, 415 (2003).
[30] M. Mrovec, D. Nguyen-Manh, D. G. Pettifor, and V. Vitek, Phys. Rev. B **69**, 094115 (2004).
[31] M. J. Cawkwell, D. Nguyen-Manh, C. Woodward, D. G. Pettifor, and V. Vitek, Science **309**, 1059 (2005).
[32] M. J. Cawkwell, D. Nguyen-Manh, D. G. Pettifor, and V. Vitek, Phys. Rev. B **73**, 064104 (2006).
[33] M. W. Finnis, *Interatomic Forces in Condensed Matter* (Oxford University Press, Oxford, 2003).
[34] A. P. Sutton, M. W. Finnis, D. G. Pettifor, and Y. Ohta, J. Phys. C **21**, 35 (1988).
[35] C. Lanczos, J. Res. Natl. Bur. Stand. **45**, 225 (1950).
[36] F. Cyrot-Lackmann, Adv. Phys. **16**, 393 (1967).
[37] K. Masuda, R. Yamamoto, and M. Doyama, J. Phys. F: Met. Phys. **13**, 1407 (1983).
[38] G. Allan, M. C. Desjonqueres, and D. Spanjaard, Solid State Commun. **50**, 401 (1984).
[39] M. Aoki, D. Nguyen-Manh, D. G. Pettifor, and V. Vitek, Prog. Mater. Sci. (to be published).
[40] P. Alinaghian, P. Gumbsch, A. J. Skinner, and D. G. Pettifor, J. Phys.: Condens. Matter **5**, 5795 (1993).
[41] R. H. Brown and A. E. Carlsson, Phys. Rev. B **32**, 6125 (1985).
[42] M. Aoki and D. G. Pettifor (unpublished).
[43] H. Hellmann, *Einführung in die Quantenchemie* (Deuticke, Leipzig, 1937).
[44] R. P. Feynman, Phys. Rev. **56**, 340 (1939).
[45] For odd values of n_{max} we could have also chosen $a_n = a_\infty$, $b_n = b_\infty$ for $n \geqslant (n_{max}-1)/2$ to keep all moments exact up to $\mu_{n_{max}}$.
[46] M. Abramowitz and I. A. Stegun, *Handbook of Mathematical Functions with Formulas, Graphs, and Mathematical Tables* (Dover, New York, 1972), Chap. 22, p. 771.
[47] R. N. Silver and H. Röder, Int. J. Mod. Phys. C **5**, 735 (1994).
[48] R. N. Silver, H. Röder, A. F. Voter, and J. D. Kress, J. Comput. Phys. **124**, 115 (1996).
[49] A. Weiße, G. Wellein, A. Alvermann, and H. Fehske, Rev. Mod. Phys. **78**, 275 (2006).
[50] N. Beer and D. G. Pettifor, in *Electronic Structure of Complex Systems*, edited by W. Temmermann (Plenum, New York, 1984), p. 769.
[51] O. K. Andersen, W. Klose, and H. Nohl, Phys. Rev. B **17**, 1209 (1978).
[52] D. G. Pettifor, J. Phys. F: Met. Phys. **7**, 613 (1977).
[53] H. Hasegawa and D. G. Pettifor, Phys. Rev. Lett. **50**, 130 (1983).
[54] E. C. Stoner, Proc. R. Soc. London, Ser. A **169**, 339 (1939).
[55] W. M. Lomer, Br. J. Appl. Phys. **12**, 535 (1961).
[56] O. Gunnarsson, J. Phys. F: Met. Phys. **6**, 587 (1976).
[57] J. Madsen, O. K. Andersen, U. K. Poulson, and O. Jepsen, in *Canonical Band Theory of the Volume and Structure Dependence of the Iron Magnetic Moment*, AIP Conf. Proc. No. 29 (AIP, New York, 1976), p. 327.
[58] D. M. Roy and D. G. Pettifor, J. Phys. F: Met. Phys. **7**, L183 (1977).
[59] H. C. Herper, E. Hoffmann, and P. Entel, Phys. Rev. B **60**, 3839 (1999).
[60] W. Zhong, G. Overney, and D. Tomanek, Phys. Rev. B **47**, 95 (1993).
[61] V. L. Moruzzi, J. F. Janak, and A. R. Williams, *Calculated Electronic Properties of Metals* (Pergamon, New York, 1978).
[62] S. L. Dudarev and P. M. Derlet, J. Phys.: Condens. Matter **17**, 7097 (2005).
[63] P. M. Derlet and S. L. Dudarev, Prog. Mater. Sci. (to be published).
[64] F. Ducastelle and F. Cyrot-Lackmann, J. Phys. Chem. Solids **32**, 285 (1971).